Crashworthiness behavior of a new rectangular thin-walled tube with Lozenge-Shaped structures under offset loading

Pouyan Tahouneh [1], Hossein Fakhri Vayqan [1], Parisa Hosseini Tehrani [1*]

[1]School of Railway Engineering, Iran University of Science and Technology, Iran, Tehran

ARTICLE INFO	ABSTRACT
	In this study, the crashworthiness of a novel rectangular energy absorber, constructed from stainless steel SUS301L-DLT, is examined under axial and offset loadings. In this task the LS-DYNA explicit nonlinear finite element is used to construct and examine the models. To validate the numerical modeling, some results are compared to the existing experimental ones. The results of the new models demonstrate a notable enhancement in crashworthiness parameters in comparison to the original model, with the energy absorption parameter exhibiting an increase of 11.23%. Notably, the presented model demonstrates stable performance under offset loading conditions of up to 45 mm displacement. Subsequently, the thickness effect of the lozenge-shaped structure is investigated considering 11 different cases. It has been demonstrated that an increase in thickness results in a higher energy absorption capacity without an accompanying increase in the initial peak force.

1. Introduction

The emergence of new technologies has spurred a significant rise in the proliferation of railway vehicles. However, this surge in railway vehicle numbers has unfortunately been accompanied by an increase in accidents and resultant injuries. Statistical data and documented evidence indicate a significant increase in the number of casualties resulting from railway accidents over the past decades [1]. One of the most prevalent types of collapsible energy absorbers is thin-walled (TW) components, which are employed extensively to absorb kinetic energy and enhance structural crashworthiness. The extensive adoption of TW tubes as energy absorbers can be attributed to a number of key factors. These encompass their superior capability to withstand dynamic load, their cost-effectiveness, high operational efficiency, and the ease of manufacturing and installation processes[2]. Various thin-walled energy absorbers are used to absorb energy and reduce damage. These include tubes [3-8], lattice

structures [9-11] and honeycombs [12-16]. Other types of energy absorbers such as novel bio-inspired fractal multi-cellular circular tubes [17], foam-filled star-shaped polygons [18] and tapered thin-walled tubes [19] can be mentioned. Side impact effectiveness is one of the most important issues in the design of energy absorption systems for rail vehicles. In this context, Xu et al [20-21] compared and optimized the crash performance of axisymmetric rectangular tube (ART) and uniform thickness tube (UTT). In the offset loading scenario, the operating range of the ART decreased more significantly than that of the UTT as the offset distance increased. Specifically, at an offset distance (d) of 45 mm, the operating ranges of the UTT and ART were reduced to 50% and 31.25% of their original ranges, respectively. The results show that, overall, the ART exhibited higher levels of Initial Peak Crushing Force (IPCF) and Specific Energy Absorption (SEA) than the UTT under the conditions tested. This suggests that the ART

may offer superior performance in terms of these critical parameters, making it a potentially more effective choice for offset loading scenarios [21]. Xing et al. [22] examined the crashworthiness optimization of a step-like energy absorber composed of nested thin-walled rectangular tubes. The step-like energy absorber, demonstrates a favorable response under axial impact loading. In comparison to the initial design, the optimal solution led to a rise in the SEA value from 8.93 to 9.36. In another study, Xu et al. [23] introduced a new double-tapered rectangular tube with diaphragms as an energy absorber. The primary focus of this study was on the geometry of the diaphragms. It was observed that the weld seam length and hole size of the diaphragm had strong effects on both the energy absorption (EA) and the specific energy absorption of the tube. In another study, Chen et al. [24] investigated a multi-cell Energy-Absorbing Structure (EAS) intended for use in high-speed trains, utilizing LS-DYNA simulation. The study focused on investigating the effects of three parameters: orthohexagonal side, side pillar and corner pillar on various crashworthiness metrics. Xu et al. [25] proposed a double-tapered rectangular tube with diaphragms. They focused on defining the thicknesses of the diaphragms and the two sets

of outer tube's symmetry faces as three design variables.

The purpose of this study is to present a new model and to investigate its stability under offset loading. The effect of the thickness of the new internal structure on the stability of the model is also discussed. Furthermore, the effects of thickness variations of the internal cell on the crashworthiness of the presented model are discussed.

2. Describing Model and methods

2.1. Describing geometric attributes

First of all, we will consider describing the outer tube of the model presented. The cross-section of this tube is 120 mm long and 94 mm wide. The thickness of the tube is 4mm. The length of the structure is divided into four sections of different length. Three diaphragms and two Lozenge-Shaped (LS) internal boxes positioned between the diaphragm (Figure 1). The distance between the diaphragms is 90mm, and the position of the first diaphragm is 50 mm from the top of the tube. The dimensions of the LS structures have been selected based on the dimensions of the tube. This design not only facilitates the formation of folds, but also
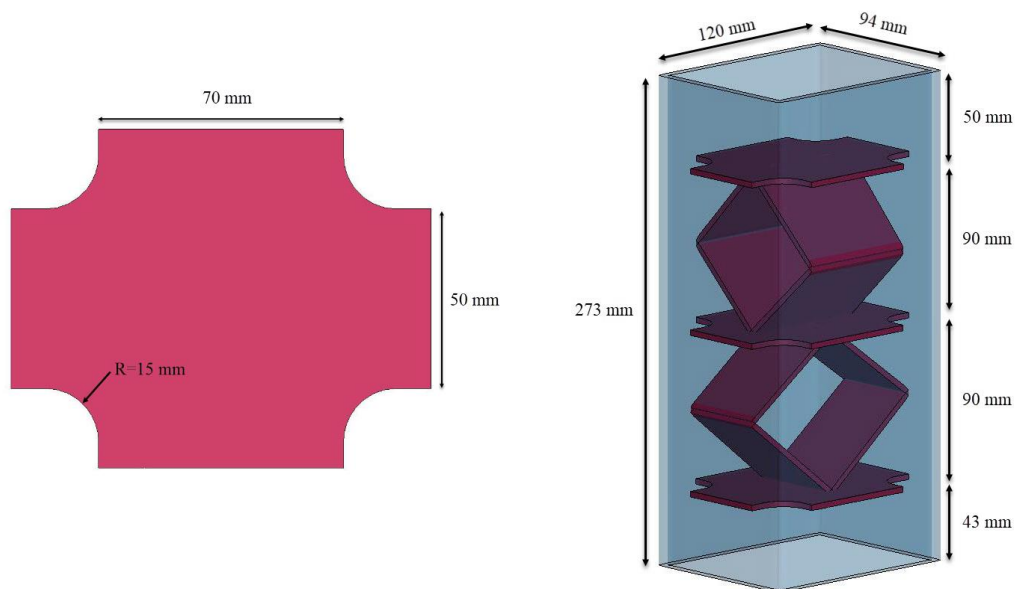

Figure 1. Dimensions of EAS and Diaphragms

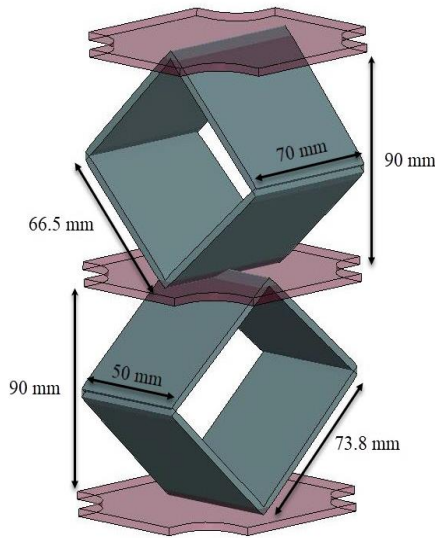enhances the energy absorption capacity of the structure (Figure 2).

Figure 2. schematic view of LS

2.2. Numerical Models

The explicit nonlinear finite element analysis code LS-DYNA is used to develop the numerical models in this study. The tube, diaphragm, and LS structures are modeled using four-node Belytschko-Tsay shell elements, while the impactor is modeled using hexahedral solid elements. It is observed that at an element size of 4 mm, the energy absorption element size curve stabilizes. Therefore, by the criteria for computationally accurate and efficient performance, the element size of the model is set at 4 mm.

In addition, the size of the impactor elements has been set at 4 mm. This part is defined as a rigid body. The tube, diaphragms, and LS structures are made of stainless steel SUS301L-DLT. The mass of the model is 6.1 kg. Its properties as an elastic linear plastic material are characterized by MAT#24 in LS-DYNA. MAT#20 properties are also used for the definition of the rigid impactor material. Detailed mechanical properties of this material and its true stress versus plastic strain curves are given in Table 1 and Figure 3 respectively [6]. The contact type "AUTOMATIC_SURFACE_TO_SURFACE" is used for the contact between the impactor and the EAS and all internal contacts between other components. The values of the static coefficient of friction and the dynamic coefficient of friction

are set to 0.3 and 0.2 respectively. The effect of strain rate is ignored and all simulations are performed under quasi-static conditions. The velocity of the impactor is kept constant at 1000 mm/s during the descent of the impactor [26], while the lower nodes are kept fixed (Figure 4).

2.3. Crashworthiness indices

When a collision occurs, the primary requirement for a crashworthy design is to absorb energy. A controlled and stable collapse pattern of an EAS is beneficial to maximize energy absorption as this allows greater amounts of energy to be absorbed. In addition, a maximum crushing force limit avoids passenger injury. To achieve optimum performance in a collision, specific structural crashworthiness indices are used. Key indices such as energy absorption, first-peak crush strength, specific energy absorption, mean crush strength (MCF) and crush load effectiveness (CLE), defined in equations (1) to (4), are commonly selected for evaluation. EA, for example, is derived from force-displacement (F-D) curves. It can be calculated using the following formula [27]:

$$EA = \int_0^S F(s)ds \qquad (1)$$

In this context, F(s) represents the instantaneous crushing force, while S represents the magnitude of the displacement during the crash.

The second index, IPCF, represents the peak value of F(s) observed during the initial phase of a collision event. This is important in assessing the likelihood of occupant survival [28].

The SEA represents the EA per unit of mass [8], which can be expressed as follows:

$$SEA = \frac{EA}{M} \qquad (2)$$

In addition, the MCF for a given deformation is a quantification of the EA capacity of a structure. As shown below, it can be calculated by dividing EA by the crushing stroke S:

$$MCF = \frac{EA}{S} \qquad (3)$$

In statistical analysis, the CLE is defined as the proportion of the ratio of the MCF to the IPCF. It is a critical parameter for assessing crushing process stability [6]. The definition of CLE is as follows:

$$\text{CLE} = \frac{\text{MCF}}{\text{IPCF}} = \frac{\text{EA}}{\text{IPCF}} \frac{1}{\text{S}} \tag{4}$$

Here, the constant stroke is set to 200 mm. As a result, the CLE is entirely dependent on the EA and IPCF ratio.

Table 1. Material Properties.

Mechanical parameters	Values
Density (kg/m³)	7850
Young's modulus (GPa)	206
Poisson's ratio	0.3
Yield stress (MPa)	335

3. FEM validation and discussion of the results

Firstly, the LS-DYNA simulation results are validated against the numerical simulation of dynamic impact data published by Xu et al [20]. The validation is performed on the force-displacement response of an axisymmetric rectangular tube with diaphragms under axial quasi-static concentric loading conditions. The thickness of both the diaphragms and the tube is set to 4 mm, following the specifications of the experimental model. The simulation is run up to a crush distance of 200 mm. In Figure 5(a), the comparison of the F-D and energy-displacement (EA-D) curves between the experiment and the simulation shows a close match.

Both sets of curves from the numerical simulation closely match those obtained from the experiment. In addition, Table 2 provides further validation, showing IPCF values of 683.930 kN and 702.822 kN for the simulation and experiment, respectively, along with corresponding EA values of 73.12 kJ and 78.15 kJ, respectively. In addition, the validation process extends to the prediction of the
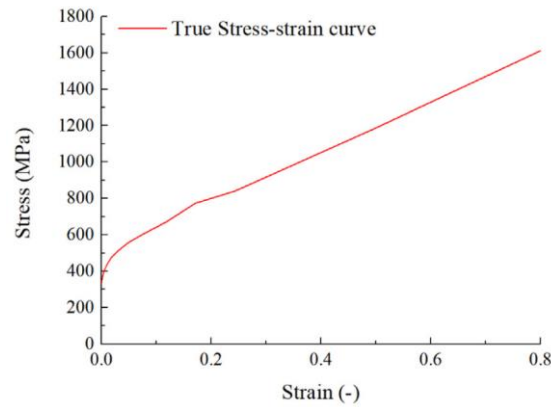

Figure 3. True stress–strain curve of the material utilized in the EAS.

deformation model. As shown in Figure 5(b), the deformation processes observed in both experiment and simulation show a high degree of agreement, further confirming the accuracy of the simulation results.

Table 2. Comparison between numerical and experimental results.

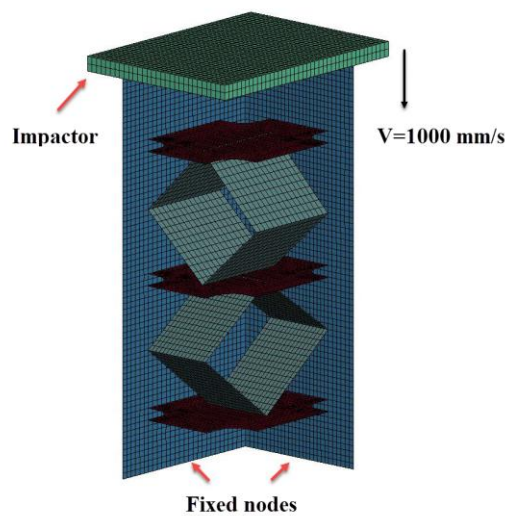|	IPCF (kN)	EA (kJ)
Numerical results	683.93	73.12
Experimental results	702.82	78.15
Error %	2.6%	6.4%

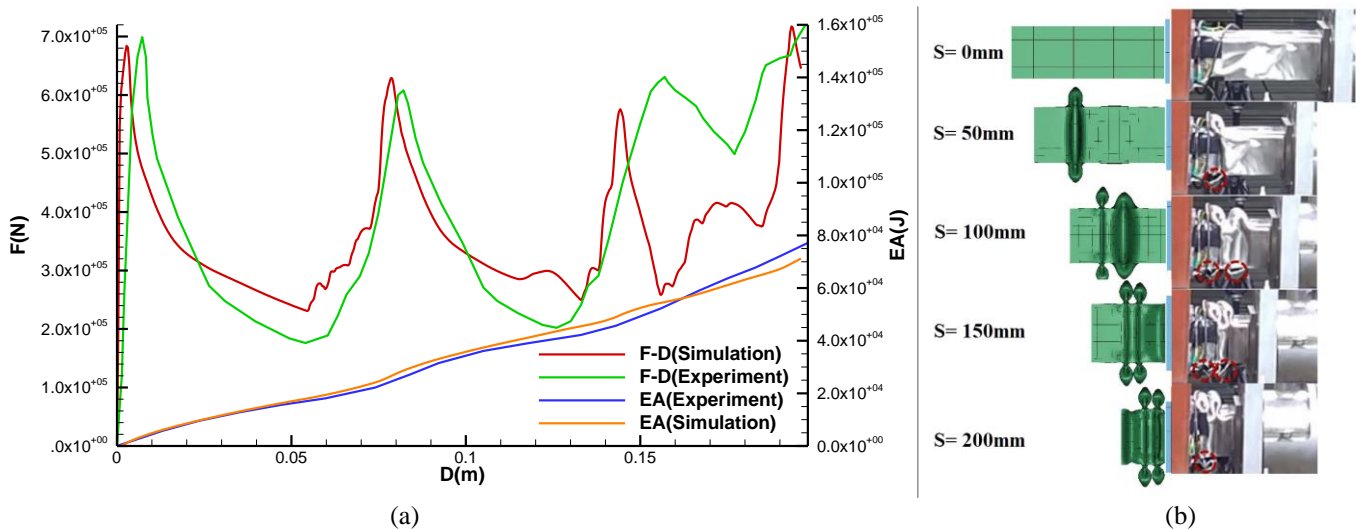Figure 4. Isometric view of FE model at quasi-static loading.

Figure 5.   (a) comparison of F-D and EA-D curves between the simulation and experiment.
(b) deformation processes of simulation and the experiment model.

4. Results

In this study, the thickness of the tube and the diaphragms are set to 5 and 3.12 mm, respectively, based on the optimization results reported by Xu et al [8]. This is an optimum condition for the maximization of energy absorption. The thickness of the LS structures is also set to be equal to the thickness of the diaphragms. In order to compare the new model with the optimal model from the aforementioned article, the simulations are subjected to both axial and vertical displacement loads according to the conditions specified in [8].

4.1. Crashworthiness capacity under axial loading

Under axial load, the EA increases by 11.23% whereas the IPCF increases by only 0.99%. In addition, the total mass of the EAS increases from 5.35 to 6.1 kg. Comparative data for the original and new models are shown in Table 3 and Figure 6.

Table 3. Performance Comparison between two EAS

	EA(KJ)	IPCF(KN)	MCF	CLE
New design with LS	119.30	928.78	596.5	0.642
Xu et al. model	107.25	919.62	536.25	0.583
Variation %	+11.23	+0.99	+11.23	+10.12
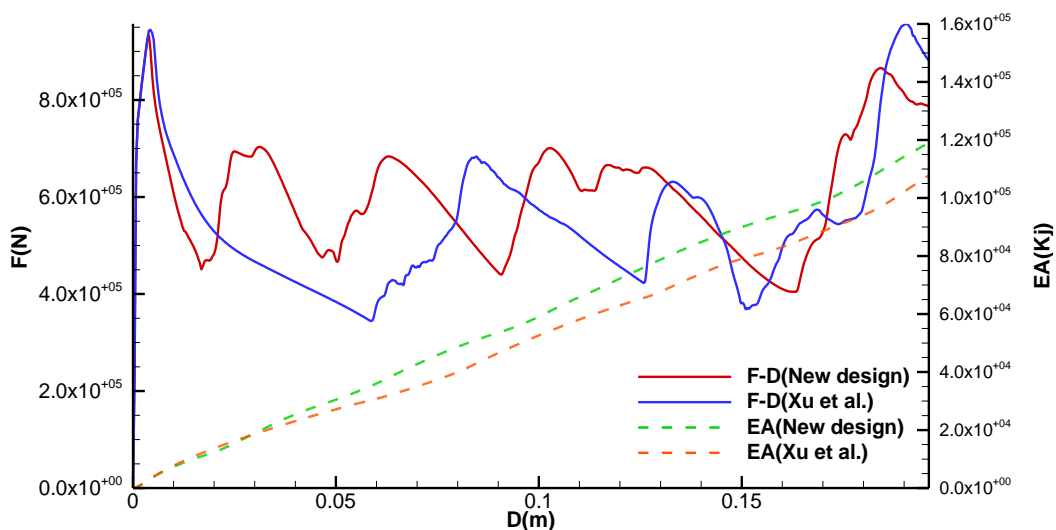
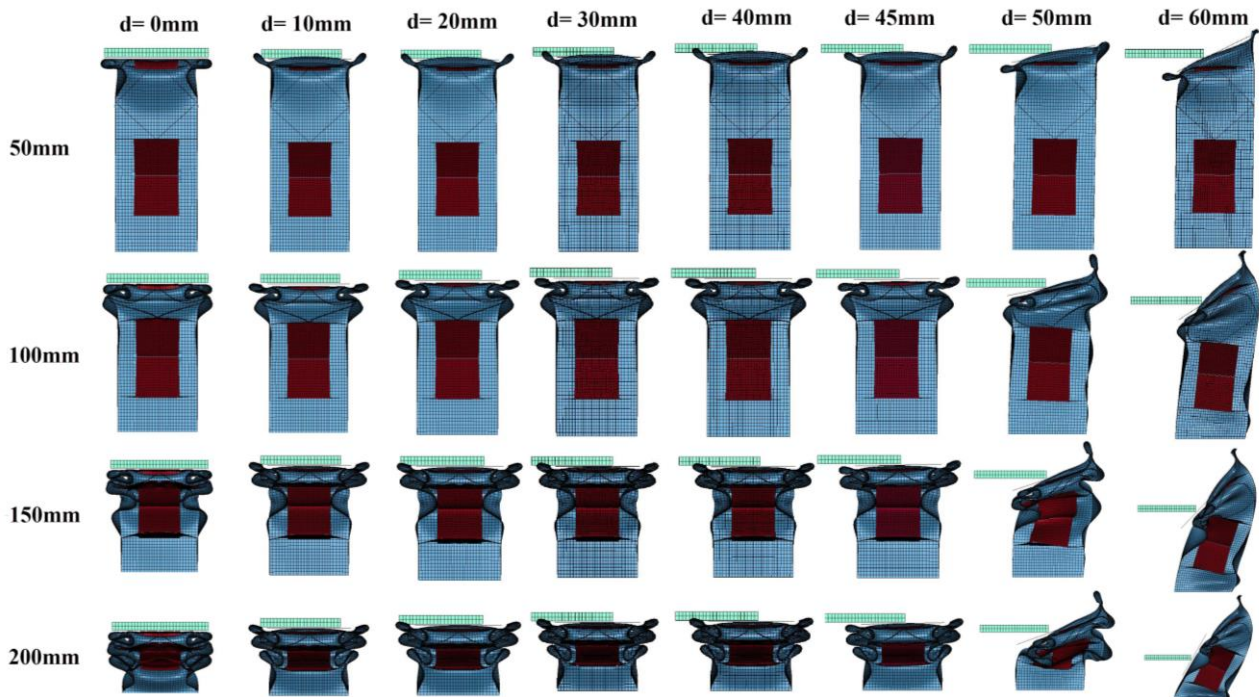Figure 6. Comparing force-displacement and energy-displacement curves.

Figure 7. The behavior of the EAS under offset loadings.

Based on the force-displacement diagram and the extracted data, the MCF parameter has increased by approximately 11%. An important point about the LS structure is that it increases overall EA without raising IPCF. This is because the LS structure not only absorbs energy through crushing but also assists in the formation of folds in the main box. When a vertical force is applied to this structure, the lateral forces generated by the deformation of the LS structure direct the main box body toward a fold formation mode. As a result, despite the increased overall stiffness of the structure, the IPCF does not significantly rise. As there has been no significant change in the IPCF, the EA increase has consequently resulted in an increase in the CLE. A higher CLE indicates that the average force is closer to the peak force, which results in a flatter F-D curve.

4.2. Crashworthiness capacity under offset loading

The EAS is required to withstand a vertical offset of 40 mm while maintaining its normal function in accordance with the EN 15227 railway crashworthiness standard [29]. On the basis of this requirement, the energy absorption of the absorber under an offset load is investigated. Simulations are performed for 10,

20, 30, 40, 50 and 60mm offsets. The observations show that the EAS remains stable under an offset load of up to 40 mm. Between offsets of 40 and 50 mm, however, the behavior of the EAS changes. Therefore, for further investigation, 45mm offset loading was added to the simulations. The EAS behavior under the 45mm offset load remains stable, as shown in Figure 7. At the 50 mm offset load, the formation of the folds is slightly disturbed, but the performance of the EAS remains acceptable. However, at 60 mm offset the EAS behavior changes from buckling to bending. It is observed that up to 40 mm offset load, the EAS behavior and energy absorption parameters remain consistent. Therefore, in Figure 8 and Table 4,

Table 4. Performance Comparison under offset loading.

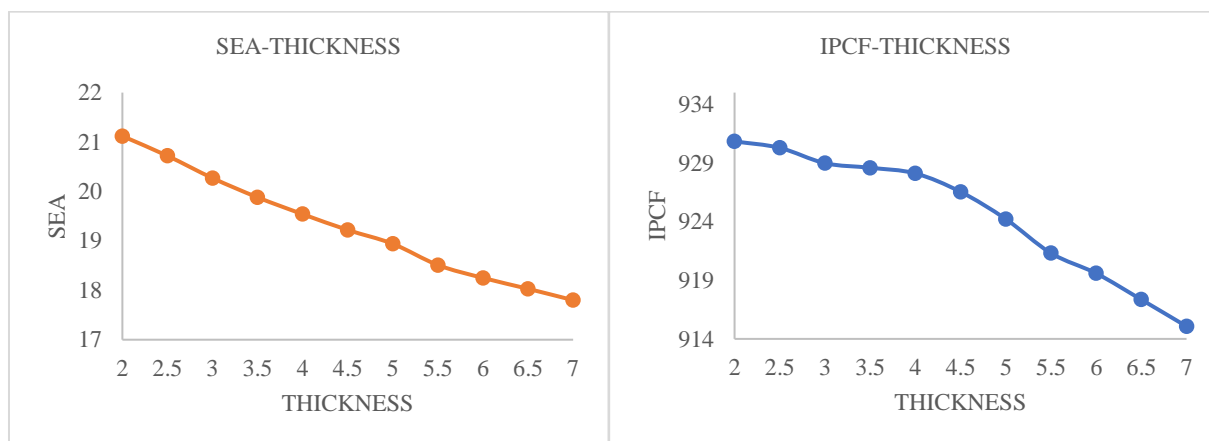| d(mm)	EA(KJ)	IPCF(KN)	SEA(KJ/Kg)
10-40	119.17	928.78	19.53
45	118.97	900.52	19.50
50	114.25	830.58	18.72
60	91.19	709.02	14.95

Figure 9. thickness effects on SEA and IPCF parameters.

Figure 8. The behavior of force-displacement curves of new EAS under offset loadings.

the results related to loading at 40 mm offset are presented, representing simulations with offsets ranging from 10 to 40 mm. The results indicate that EA and IPCF exhibit minimal variation up to a 45 mm offset loading. At the 50 mm offset load, due to the formation of an unstable fold, there is a decrease in EA, although the structure still demonstrates acceptable performance. At an offset load of 60 mm, there is a decrease of approximately 11% in EA, and the F-D graph demonstrates a gradual decline in the structure's energy absorption over time.

4.3. LS thickness effects on crashworthiness parameters

A parametric study is carried out to investigate the effect of the thickness of the LS structure on the energy absorption parameters. The thickness of the LS structure is varied from 2 to 7 mm in this section. The results of the simulations are shown in Table 5.

The results show that IPCF decreases by 1.7% as the thickness of the LS structure increases. The fact that the first fold formed is outside the area of the LS structure explains the lack of significant change in this parameter. Also, as the thickness increases, the amount of EA increases by 4.9%, but because the total mass of the structure increases greatly as the thickness increases, the SEA parameter decreases by 15.7% (Figure 9). Therefore, if the mass

parameter is a consideration in the design of the structure, lower thicknesses should be used.

5. Conclusions

In this study, we presented a new design by adding a lozenge-shaped structure to an initial model. A principal feature of the LS structure is that it facilitates enhanced overall energy absorption without an increase in the initial peak crushing force.

Firstly, there was a validation of the FEM model with experimental test results. Then, we compared the Energy Absorbed Parameters with those obtained using the original model. The next step was to investigate the presented model under an offset load. Finally, there was an investigation of the effect of the thickness of the LS structure on the energy absorption parameters. The following conclusions are obtained:

- When considering the LS structure under axial loading in comparison to the model of Xu et al., the EA increases by 11.23%, while the IPCF increases by 0.99%. In addition, based on the force-displacement diagram and the extracted data, the MCF parameter increases by approximately 11%, while the CLE parameter increases by 10%. The higher achieved CLE is an indication that the average force is closer to the peak force.

- Observations show that the EAS remains stable up to 45 mm offset load when considering the LS structure under offset load. It is observed that the behavior of the EAS and the energy absorption parameters remain consistent up to an offset load of 40 mm. At an offset load of 50 mm, the formation of wrinkles is slightly disturbed, but the performance of the EAS remains acceptable. Nevertheless, at an offset of 60 mm, the EA is observed to decrease by 10.9%. Furthermore, the force-deflection (F-D) graph indicates a gradual reduction in the EA over time, due to the transition in the behavior of the EAS from buckling to bending.
- The investigation of the thickness of the LS structure shows that the amount of IPCF is almost constant with variation of this parameter. Also, as the thickness increases, the amount of EA increases by 4.9%, but the SEA parameter decreases by 15.7%. Therefore, if the mass parameter is one of the considerations in the design of the structure, a lower thickness should be chosen.

References

[1] G. (Guoxing) Lu and T. X. (Tongxi) Yu, *Energy absorption of structures and materials*. CRC Press, 2003.

[2] A. Baroutaji, M. Sajjia, and A. G. Olabi, "On the crashworthiness performance of thin-walled energy absorbers: Recent advances and future developments," *Thin-Walled Structures*, vol. 118. Elsevier Ltd, pp. 137–163, Sep. 01, 2017. doi: 10.1016/j.tws.2017.05.018.

[3] P. Xu *et al.*, "Theoretical development and multi-objective optimization of a double-tapered rectangular tube with diaphragms," *International Journal of Crashworthiness*, vol. 27, no. 1, pp. 206–220, 2022, doi: 10.1080/13588265.2020.1785109.

[4] J. Chen, P. Xu, S. Yao, J. Xing, and Z. Hu, "The multi-objective structural optimization design to improve the crashworthiness of a multi-cell structure for a high-speed train," *International Journal of Crashworthiness*, vol. 27, no. 1, pp. 24–33, 2022, doi: 10.1080/13588265.2020.1773739.

[5] P. Xu *et al.*, "Optimisation of double-tapered rectangular tube with O-shaped diaphragms as energy absorber," *International Journal of Crashworthiness*, vol. 27, no. 3, pp. 651–660, 2022, doi: 10.1080/13588265.2020.1836786.

[6] P. Xu *et al.*, "Parameter study and multi-objective optimization of an axisymmetric rectangular tube with diaphragms for subways," *Thin-Walled Structures*, vol. 136, pp. 186–199, Mar. 2019, doi: 10.1016/j.tws.2018.12.025.

[7] J. Xing *et al.*, "Crashworthiness optimisation of a step-like bi-tubular energy absorber for subway vehicles," *International Journal of Crashworthiness*, vol. 25, no. 3, pp. 252–262, May 2020, doi: 10.1080/13588265.2019.1577522.

[8] K. Xu *et al.*, "Crashworthiness optimisation for the rectangular tubes with axisymmetric and uniform thicknesses under offset loading," *Structural and Multidisciplinary Optimization*, vol. 62, no. 2, pp. 957–977, Aug. 2020, doi: 10.1007/s00158-020-02535-1.

[9] X. Wang, R. Qin, X. Zhang, and B. Chen, "Quasi-static and dynamic behavior of additively manufactured metamaterial structures with layered-hybrid topologies," *Thin-Walled Structures*, vol. 183, Feb. 2023, doi: 10.1016/j.tws.2022.110434.

[10] X. Wang, R. Qin, and B. Chen, "Crashworthiness reinforcements of multi-cell thin-walled tubes through topology optimized lattice structures

under axial and lateral loadings," *Mechanics of Advanced Materials and Structures*, vol. 30, no. 18, pp. 3662–3686, 2023, doi: 10.1080/15376494.2022.2081390.

[11] A. Baykasoğlu, C. Baykasoğlu, and E. Cetin, "Multi-objective crashworthiness optimization of lattice structure filled thin-walled tubes," *Thin-Walled Structures*, vol. 149, Apr. 2020, doi: 10.1016/j.tws.2020.106630.

[12] G. Zhu, S. Li, G. Sun, G. Li, and Q. Li, "On the design of graded honeycomb filler and tubal wall thickness for multiple load cases," *Thin-Walled Structures*, vol. 109, pp. 377–389, Dec. 2016, doi: 10.1016/j.tws.2016.09.017.

[13] Z. Wang, H. Tian, Z. Lu, and W. Zhou, "High-speed axial impact of aluminum honeycomb - Experiments and simulations," *Compos B Eng*, vol. 56, pp. 1–8, 2014, doi: 10.1016/j.compositesb.2013.07.013.

[14] Z. Wang, S. Yao, Z. Lu, D. Hui, and L. Feo, "Matching effect of honeycomb-filled thin-walled square tube—Experiment and simulation," *Compos Struct*, vol. 157, pp. 494–505, Dec. 2016, doi: 10.1016/j.compstruct.2016.03.045.

[15] H. Mozafari, S. Khatami, H. Molatefi, V. Crupi, G. Epasto, and E. Guglielmino, "Finite element analysis of foam-filled honeycomb structures under impact loading and crashworthiness design," *International Journal of Crashworthiness*, vol. 21, no. 2, pp. 148–160, Mar. 2016, doi: 10.1080/13588265.2016.1140710.

[16] Z. Wang, J. Liu, Z. Lu, and D. Hui, "Mechanical behavior of composited structure filled with tandem honeycombs," *Compos B Eng*, vol. 114, pp. 128–138, Apr. 2017, doi: 10.1016/j.compositesb.2017.01.018.

[17] N. S. Ha, T. M. Pham, W. Chen, H. Hao, and G. Lu, "Crashworthiness analysis of bio-inspired fractal tree-like multi-cell circular tubes under axial crushing," *Thin-Walled Structures*, vol. 169, Dec. 2021, doi: 10.1016/j.tws.2021.108315.

[18] S. Goyal, C. S. Anand, S. K. Sharma, and R. C. Sharma, "Crashworthiness analysis of foam filled star shape polygon of thin-walled structure," *Thin-Walled Structures*, vol. 144, Nov. 2019, doi: 10.1016/j.tws.2019.106312.

[19] E. Acar, M. A. Guler, B. Gereker, M. E. Cerit, and B. Bayram, "Multi-objective crashworthiness optimization of tapered thin-walled tubes with axisymmetric indentations," *Thin-Walled Structures*, vol. 49, no. 1, pp. 94–105, Jan. 2011, doi: 10.1016/j.tws.2010.08.010.

[20] P. Xu *et al.*, "Parameter study and multi-objective optimisation of an axisymmetric rectangular tube with diaphragms for subways," *Thin-Walled Structures*, vol. 136, pp. 186–199, Mar. 2019, doi: 10.1016/j.tws.2018.12.025.

[21] K. Xu *et al.*, "Crashworthiness optimisation for the rectangular tubes with axisymmetric and uniform thicknesses under offset loading," *Structural and Multidisciplinary Optimization*, vol. 62, no. 2, pp. 957–977, Aug. 2020, doi: 10.1007/s00158-020-02535-1.

[22] J. Xing *et al.*, "Crashworthiness optimisation of a step-like bi-tubular energy absorber for subway vehicles," *International Journal of Crashworthiness*, vol. 25, no. 3, pp. 252–262, May 2020, doi: 10.1080/13588265.2019.1577522.

[23] P. Xu *et al.*, "Optimisation of double-tapered rectangular tube with O-shaped diaphragms as energy

absorber," *International Journal of Crashworthiness*, vol. 27, no. 3, pp. 651–660, 2022, doi: 10.1080/13588265.2020.1836786.

[24] J. Chen, P. Xu, S. Yao, J. Xing, and Z. Hu, "The multi-objective structural optimisation design to improve the crashworthiness of a multi-cell structure for high-speed train," *International Journal of Crashworthiness*, vol. 27, no. 1, pp. 24–33, 2022, doi: 10.1080/13588265.2020.1773739.

[25] P. Xu *et al.*, "Theoretical development and multi-objective optimisation of a double-tapered rectangular tube with diaphragms," *International Journal of Crashworthiness*, vol. 27, no. 1, pp. 206–220, 2022, doi: 10.1080/13588265.2020.1785109.

[26] X. Zhang and H. Zhang, "Crush resistance of square tubes with various thickness configurations," *Int J Mech Sci*, vol. 107, pp. 58–68, Mar. 2016, doi: 10.1016/j.ijmecsci.2016.01.003.

[27] X. Song, G. Sun, G. Li, W. Gao, and Q. Li, "Crashworthiness optimization of foam-filled tapered thin-walled structure using multiple surrogate models," *Structural and Multidisciplinary Optimization*, vol. 47, no. 2, pp. 221–231, Feb. 2013, doi: 10.1007/s00158-012-0820-6.

[28] P. Xu, C. Yang, Y. Peng, S. Yao, J. Xing, and B. Li, "Cut-out grooves optimization to improve crashworthiness of a gradual energy-absorbing structure for subway vehicles," *Mater Des*, vol. 103, pp. 132–143, Aug. 2016, doi: 10.1016/j.matdes.2016.04.059.

[29] "En 15227".